INSTITUTE OF PHYSICS PUBLISHING and INTERNATIONAL ATOMIC ENERGY AGENCY NUCLEAR FUSION

Nucl. Fusion **46** (2006) S868–S879 doi:10.1088/0029-5515/46/10/S02

Alfvén cascades in JET discharges with NBI-heating

S.E. Sharapov[1], B. Alper[1], Yu.F. Baranov[1], H.L. Berk[2], D. Borba[3], C. Boswell[4], B.N. Breizman[2], C.D. Challis[1], M. de Baar[5], E. De La Luna[6], E.A. Evangelidis[7], S. Hacquin[3], N.C. Hawkes[1], V.G. Kiptily[1], S.D. Pinches[8], P. Sandquist[9], I. Voitsekhovich[1], N.P. Young[1,10] and JET-EFDA Contributors[a]

[1] Euratom/UKAEA Fusion Association, Culham Science Centre, Abingdon OX14 3DB, UK
[2] Institute Fusion Studies, University of Texas at Austin, Austin, USA
[3] Euratom/IST Fusion Association, Centro de Fusao Nuclear, Lisboa, Portugal
[4] PSFC, Massachussets Institite of Technology, Cambridge, USA
[5] Association Euratom-FOM Institute Plasmaphysics 'Rijnhuizen', Nieuwegein, The Netherlands
[6] Association Euratom-CIEMAT, Lab. National de Fusion, Madrid, Spain
[7] Euratom/Helenic Fusion Assoc., Democritos University of Thrase, Xanthi, Greece
[8] Max Planck Institute fur Plasmaphysik, Euratom Association, Garching, Germany
[9] Euratom/VR Fusion Association, Chalmers University of Technology, Goteborg, Sweden
[10] University of Warwick, Coventry, UK

E-mail: sergei.sharapov@jet.uk

Received 28 March 2006, accepted for publication 26 April 2006
Published 18 September 2006
Online at stacks.iop.org/NF/46/S868

Abstract
Alfvén cascade (AC) eigenmodes excited by energetic ions accelerated with ion-cyclotron resonance heating in JET reversed-shear discharges are studied experimentally in high-density plasmas fuelled by neutral beam injection (NBI) and by deuterium pellets. The recently developed O-mode interferometry technique and Mirnov coils are employed for detecting ACs. The spontaneous improvements in plasma confinement (internal transport barrier (ITB) triggering events) and grand ACs are found to correlate within 0.2 s in JET plasmas with densities up to $\sim 5 \times 10^{19}\,\mathrm{m}^{-3}$. Measurements with high time resolution show that ITB triggering events happen before 'grand' ACs in the majority of JET discharges, indicating that this improvement in confinement is likely to be associated with the decrease in the density of rational magnetic surfaces just before $q_{\min}(t)$ passes an integer value. Experimentally observed ACs excited by sub-Alfvénic NBI-produced ions with parallel velocities as low as $V_{\|\mathrm{NBI}} \approx 0.2 \cdot V_{\mathrm{A}}$ are found to be most likely associated with the geodesic acoustic effect that significantly modifies the shear-Alfvén dispersion relation at low frequency. Experiments were performed with a tritium NBI-blip (short time pulse) into JET plasmas with NBI-driven ACs. Although considerable NBI-driven AC activity was present, good agreement was found both in the radial profile and in the time evolution of DT neutrons between the neutron measurements and the TRANSP code modelling based on the Coulomb collision model, indicating the ACs have at most a small effect on fast particle confinement in this case.

PACS numbers: 52.55.Fa, 42.87.Bg, 52.35.Bj, 52.55.Hc

(Some figures in this article are in colour only in the electronic version)

1. Introduction

Several types of Alfvén instabilities are excited on JET by resonant interaction between the shear Alfvén wave and energetic ions either accelerated with ion-cyclotron resonance frequency (ICRF) heating or produced by neutral beam injection (NBI) (see, e.g. [1, 2] and references therein). JET 'advanced' plasmas with a non-monotonic safety factor profile $q(r)$ exhibit instability of Alfvén cascade (AC) eigenmodes excited by ICRH-accelerated ions [1, 3–5] or by NBI-produced ions [6], in addition to the well-known toroidal Alfvén

[a] See the appendix of J. Pamela *et al Proc. 20th IAEA Fusion Energy Conf. 2004 (Vilamoura, 2004)* (Vienna: IAEA).

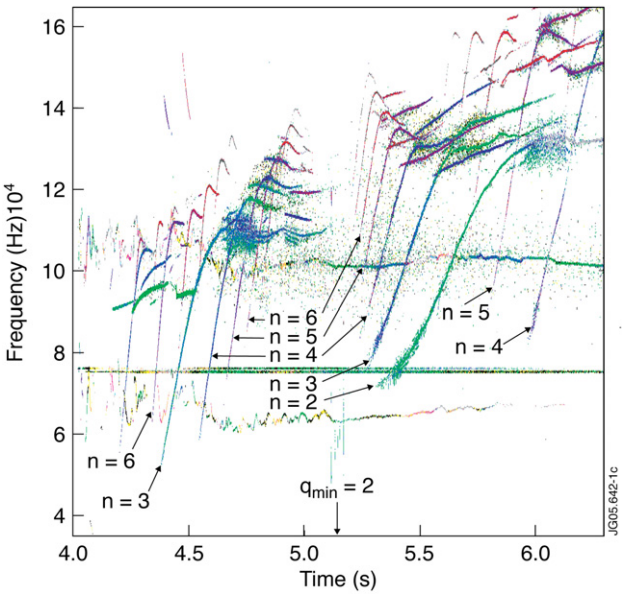

Figure 1. Magnetic spectrogram (Fourier decomposition of Mirnov coil signal) showing an example of ICRH-driven ACs with different toroidal mode numbers in a JET reversed shear plasma.

eigenmodes (TAEs) [7]. The AC eigenmode, an example of which is shown in figure 1, is a shear-Alfvén eigenmode associated with the extremum point of the Alfvén continuum localized at the magnetic surface with the minimum value of $q(r)$, labelled as $q_{\min}$ [1, 3–6, 8–10]. During the evolution of plasma current, the eigenfrequency of the AC, $\omega_{AC}(t)$, changes due to the evolution of $q_{\min}(t)$, via the relation for shear Alfvén waves,

$$\omega_{AC}(t) = \frac{V_A}{R_0}\left|n - \frac{m}{q_{\min}(t)}\right| + \Delta\omega. \qquad (1)$$

Here, n and m are the toroidal and poloidal mode numbers, R_0 is the major radius of the tokamak, $V_A = B_0/(4\pi\rho_0)^{1/2}$ is the Alfvén speed, B_0 is the equilibrium magnetic field and ρ_0 is the mass density of the plasma. The value $\Delta\omega$ in equation (1), which marks a deviation of the AC frequency from the shear Alfvén continuum, is caused by the effects of large ion orbits [4,8], toroidicity [9], thermal plasma pressure gradient [10] and deformation of the continuum itself due to a thermal plasma pressure effect [10]. It may consitute a significant part (up to one-third or half) of the maximum AC frequency, but it remains constant on a time scale of $q_{\min}(t)$ evolution. One may also note that in discharges with changing $V_A(t)$, the time dependence of $V_A(t)$ is less important than that of $q_{\min}(t)$ in equation (1) as $q_{\min}^{-1}(t)$ is multiplied by a large number m, whereas the quantity $|n - mq_{\min}^{-1}(t)|$ in front of $V_A(t)$ does not exceed $1/2q_{\min}$, the value at which the AC frequency reaches the toroidal Alfvén eigenmode (TAE) frequency. It follows from equation (1) that the AC frequency tracks the evolution of $q_{\min}(t)$ in time through

$$\frac{d}{dt}\omega_{AC}(t) \approx m\frac{V_A}{R_0}\frac{d}{dt}q_{\min}^{-1}(t), \qquad (2)$$

so that the slope in the mode frequency seen in figure 1 depends on the evolution of $q_{\min}(t)$ and for ACs with higher poloidal mode numbers m this slope is steeper. To understand what causes multiple ACs to occur simultaneously (as figure 1 shows at $t \approx 5.2$ s), one can look at equation (1) that shows that ACs with different toroidal mode numbers appear at different times, i.e. an $n = 1$ AC appears when $q_{\min}(t)$ passes integer values, $q_{\min}(t) = 1, 2, 3, \ldots$, an $n = 2$ AC appears when $q_{\min}(t)$ passes integer and half-integer values, $q_{\min}(t) = 1, 3/2, 2, 5/2, 3, \ldots$, and so on. The Alfvén cascade, in which modes with all toroidal mode numbers, n, are present, such as in figure 1 at $t \approx 5.2$ s, is called a grand cascade. The grand cascade occurs when $q_{\min}(t)$ passes an integer value while evolving from a higher to a lower value during plasma current increase.

ACs were also observed on the tokamaks JT-60U [11, 12], C-MOD [13], TFTR [14] and DIII-D [15]. Energetic ions driving the AC instability were accelerated by ICRH on JET [1], JT-60U [11] and C-MOD [13], while NBI-produced ions drove this instability in JET [6], JT-60U [12] and DIII-D [15] experiments. Fusion-born alpha-particles excited the AC modes in TFTR DT plasmas [14], confirming the importance of such instabilities for burning plasma experiments [16].

Although AC instabilities are observed in almost every JET discharge with ICRH, the amplitudes of the Alfvén perturbations saturate at relatively low values (a typical perturbed poloidal magnetic field $\delta B/B_0 \cong 10^{-6}$–$10^{-5}$ at the edge), and JET does not experience degradation of fast ion confinement associated with ACs. On the other hand, the measured discrete spectrum of ACs was found to be useful for MHD spectroscopy [17, 18] which yields information about both fast ions and MHD characteristics of plasmas [3, 19]. The most important aspect of the MHD spectroscopy based on detecting ACs in reversed-shear plasmas is the relation between the grand cascades, integer values of $q_{\min}(t)$ and so-called internal transport barrier (ITB) triggering events [20]. The relation between grand ACs and a spontaneous improvement in fusion performance was observed on JET from the very first observations of ACs. Figure 2 shows an example of such a case where the neutron rate in JET discharge was constant for about 1 s at fixed power of NBI and ICRH. However, this neutron yield was almost doubled suddenly at $t \approx 7$ s without a change in either NBI or ICRH power. At the same time, a grand cascade marking the appearance of a $q_{\min}(t) = \textit{integer}$ magnetic surface was detected with Mirnov coils at about the same time, $t \approx 7$ s. Two questions arise here: is the correlation between the improvement in fusion performance and the grand AC just a coincidence? If not can one make use of this correlation for developing scenarios with high fusion performance?

Numerous JET reversed-shear experiments have demonstrated a close link between ITBs and *low-order* rational values of $q_{\min}(t)$ [20], with *integer* $q_{\min}(t)$ surfaces most prominently linked to the ITB [20]. The link manifests itself as an ITB triggering event, which is observed, e.g. on the electron temperature profile $T_e(r,_t)$, as an increase in the slope dT_e/dr in the vicinity of $q_{\min}$. The ITB triggering event happens when $q_{\min}(t)$ approaches/passes integer value and the ITB triggering event either decays in few hundred milliseconds or develops an ITB if the main heating has been applied shortly before the ITB triggering event. The link between ITB triggering events and integer $q(r)$-values plays an important role in developing an ITB scenario on JET and it may become an important factor in developing an ITB scenario on ITER [16].

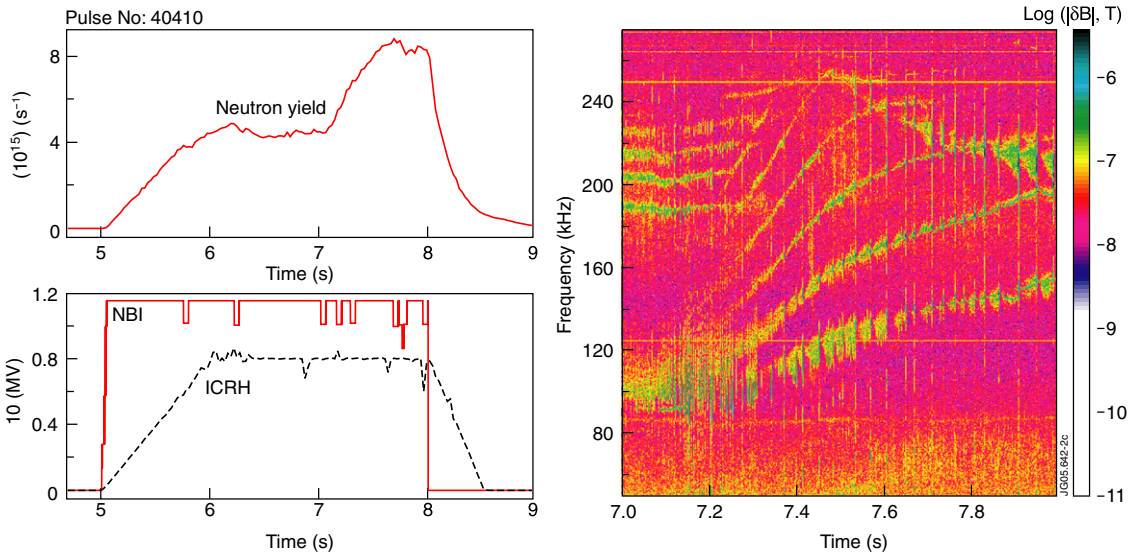

Figure 2. Left: neutron yield, NBI and ICRH power in JET discharge #40410 with toroidal magnetic field $B_T = 3.4$ T and plasma current $I_P = 3$ MA. Right: a grand cascade observed at the time of the neutron rate and T_e increase.

In order to benefit from the ITB triggering event, the main heating power is applied on JET just before $q_{min}(t) = integer$ occurs in order to maximize the possibility of triggering an ITB. During the inductive current ramp-up phase shown in figure 3(*a*), the safety factor profile $q(r, t)$ passes through a set of profiles, shown in figure 4. The 'target' $q(r)$-profile is selected which has $q_{min}(t) = integer$ just after the time when the main heating power, e.g. NBI-heating shown in figure 3(*b*), starts. After the main heating is applied, the resistive diffusion time increases significantly and the evolution of $q(r, t)$ becomes much slower than the time scale of the ITB formation. Lower hybrid current drive (LHCD) and/or ion-cyclotron resonance frequency (ICRF) heating of low power ($\leqslant$2 MW) are often employed on JET to adjust $q(r, t)$ as required at the early pre-heating phase of the discharge [21].

A reliable diagnosis of the times when $q_{min}(t)$ passes integer values plays an important role in the development of JET reversed-shear ITB scenarios as it provides a time-saving alternative to the 'timing scan' procedure, in which the time of the main heating is scanned in a sequence of discharges (as figures 3 and 4 show) in order to vary and optimize the target $q(r)$-profile. However, use of the best diagnostic tool measuring the safety factor, the motional stark effect (MSE) diagnostic [22], is somewhat inhibited as the low plasma density typical for the early phase of discharges causes significant shine-through of the diagnostic NBI. MHD spectroscopy based on detecting Alfvén cascade (AC) eigenmodes excited by ICRH-accelerated fast ions was found on JET to be a more accurate and convenient diagnostic tool for determining the most favourable times when the main heating power should be applied [20]. The grand cascade shows such a distinctive pattern on a Fourier spectrogram of the signal of plasma perturbation in the Alfvén frequency range that it is recognizable at the early phase of the discharge under very different plasma conditions and at a very low signal-to-noise ratio.

The technique of ITB triggering by low-order $q_{min}(t)$ rational surfaces was also confirmed recently on DIII-D [23, 24]. It was, however, noted that such a link seems to weaken in discharges with higher plasma density, so a problem may arise if one applies the JET technique of ITB development based on grand ACs to higher density machines, such as C-MOD or ITER. To clarify the density dependence of the link between the ITB triggering events and grand cascades, marking the times of $q_{min}(t) = integer$, the present paper considers the ITB triggering and ACs in JET discharges with high density plasmas obtained with NBI fuelling and with combined NBI fuelling and injection of pellets. Section 2 describes the main parameters of the NBI system on JET and analyses typical observations of ACs in JET discharges with high power NBI heating. It is shown in section 2 that the detection of ACs with external magnetic pick-up coils in JET discharges with high power NBI-heating is significantly obscured by a high level of magnetic noise and a weakening of the AC signal. A novel method of detecting the ACs with the use of microwave interferometry, more relevant for detecting ACs in NBI-heated JET discharges, is described. Section 3 presents a statistical analysis of the link between the ACs and the ITBs in JET discharges with plasma densities up to $\sim 5 \times 10^{19}$ m^{-3}. AC detection by the interferometry with high time resolution is then used for analysing the time sequence of ITB triggering events and grand cascades. A new phenomenon of ACs excited by sub-Alfvénic NBI is described in section 4. Experiments on the tritium blip NBI in the presence of the NBI-driven ACs are then described, and a comparison is made between the experimentally measured DT neutron yield and the TRANSP code modelling based on Coulomb collisions. A summary is given in section 5.

2. Detecting Alfvén cascades with Mirnov coils and interferometry in reversed-shear JET discharges

The NBI system on JET is capable of delivering powers in excess of 20 MW for up to 10 s duration, and it plays a major role in plasma heating and fuelling. Figure 5 shows the geometry of the NBI-heating system on JET, which consists of

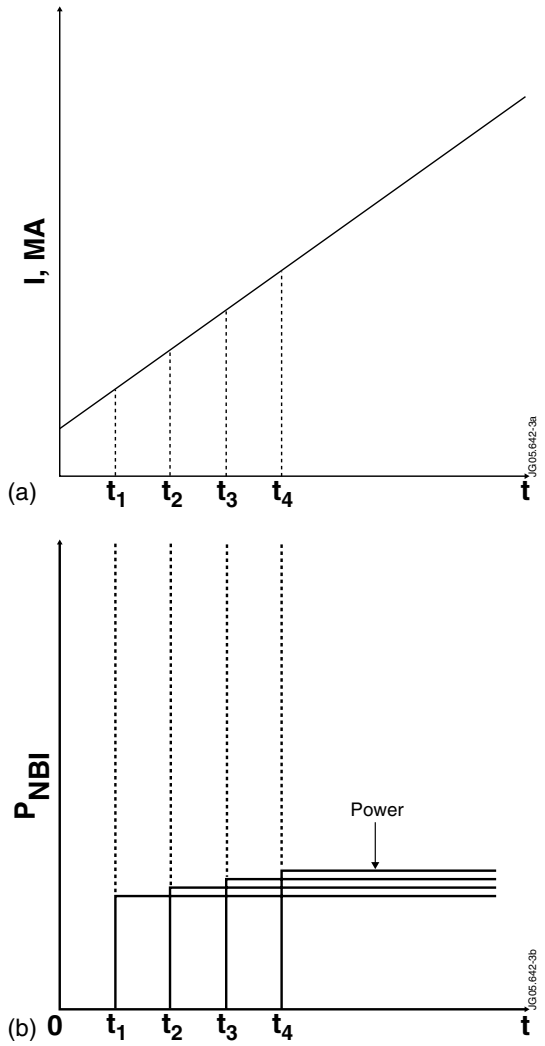

Figure 3. Schematic figure showing (*a*) the inductive current ramp-up in time and (*b*) main NBI heating power applied at different times.

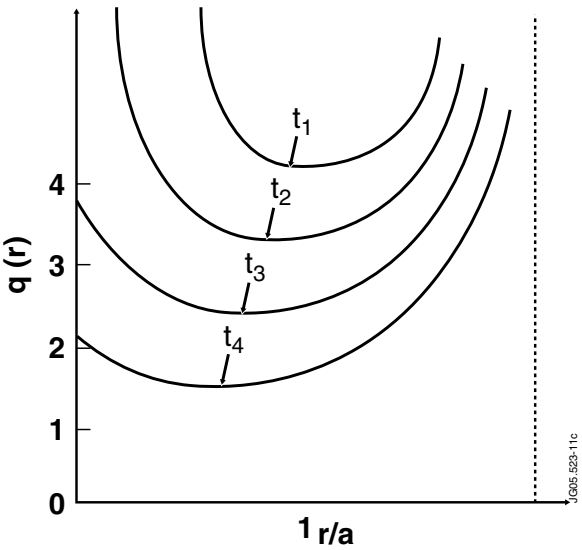

Figure 4. Schematic target $q(r)$-profiles corresponding to different times of the main heating start shown in figure 3.

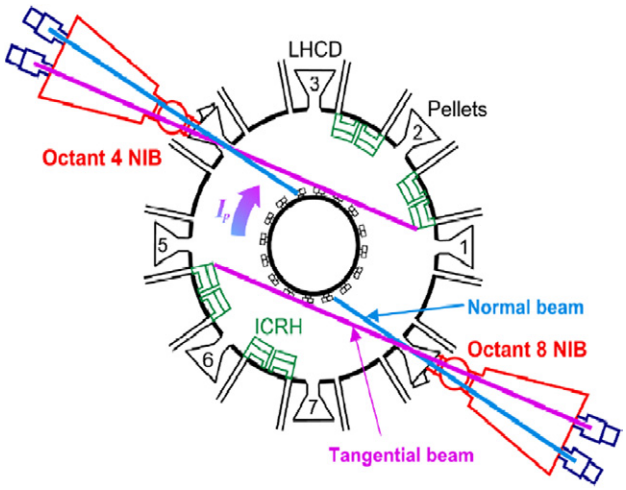

Figure 5. Geometry of the NBI injection system on JET (view from the top of the machine).

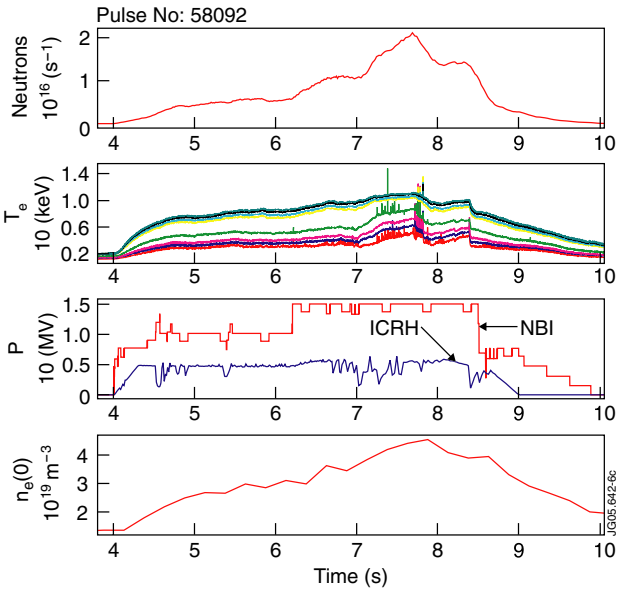

Figure 6. Time evolution of neutron rate R_{nt}, T_e, NBI and ICRH power and $n_e(0)$ in a JET reversed shear discharge with $B_T = 3.45$ T, $I_P = 3$ MA (pulse #58092).

two types of sources, nominally 80 and 130 keV. The angles of the beam trajectories to the magnetic axis are 52° and 64° for the tangential and normal banks, respectively, with the toroidal projection of the beams co-directed with the normal current direction. The unbalanced NBI can drive very high toroidal plasma rotation with frequencies up to ∼45 kHz, which adds a large Doppler shift to the frequency of modes observed on JET, such as TAEs or ACs [3].

In the presence of high-power NBI, observation of ACs excited with ICRH and detected with Mirnov coils becomes difficult. Figure 6 shows time traces of the JET reversed discharge (pulse #58092) in which the ICRH power driving the ACs was ∼4 MW, i.e. half the power of the example shown in figure 2. Spectrograms of the perturbed poloidal magnetic field, $\partial(\delta B_{AC}^{edge})/\partial t$, measured with the external Mirnov coils in this discharge, are shown in figure 7(*a*) (amplitude of the perturbation) and figure 7(*b*) (phase of the perturbation that

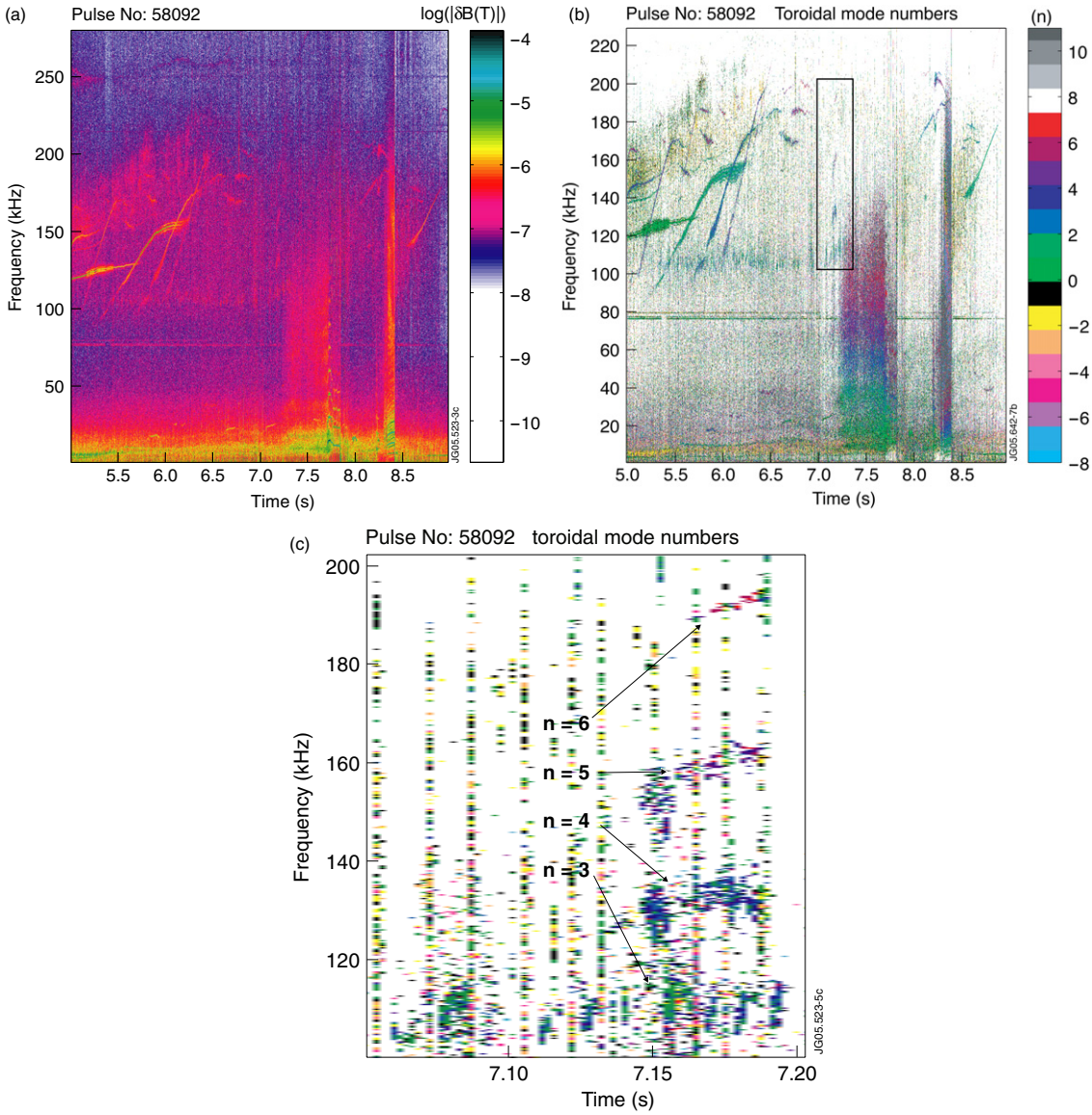

Figure 7. (*a*) Magnetic spectrogram showing weakening of AC amplitude in the high-performance phase of discharge shown in figure 6. (*b*) Strong magnetic noise is observed on the phase spectrogram showing toroidal mode numbers of the perturbations when ITB is triggered at $t \sim 7$ s. (*c*) Grand cascade of poor signal-to-noise ratio is observed at $t \sim 7$ s.

determines toroidal mode numbers). ACs are observed indeed in figures 7(*a*) and (*b*) before and after the maximum NBI power phase. However, the very high level of magnetic noise arising in figure 7(*b*) after the formation of the ITB at $t \approx 7$ s (seen as an increase in the neutron yield and electron temperature in figure 6), significantly obscures the detection of ACs during the maximum NBI power phase. Figure 7(*c*) shows an enlargement of figure 7(*b*), where a weak amplitude grand AC can just be recognized, but this would not be satisfactory as a q-profile diagnostic. Alternative ways of detecting the ACs are highly desirable for such discharges, and these were sought in dedicated JET experiments [5].

Detecting the ACs with the use of O-mode interferometry was found to be one of the most promising detection techniques on JET [5, 25]. Figure 8 (top) shows time traces of the input power and the plasma parameters from a dedicated JET discharge ($B_T \approx 2.75$ T, $I_P \approx 1.7$ MA), in which lower hybrid current drive (LHCD) was applied during the current ramp-up phase in order to obtain a reversed-shear magnetic configuration. ICRH power was used for accelerating hydrogen minority ions to energies high enough for the ions to resonate with shear Alfvén waves. The reflectometer/interferometer on JET is located at the outer side of the torus (at major radius $R \approx 4$ m) and it views the plasma horizontally through the magnetic axis with the line-of-sight perpendicular to the magnetic axis, as figure 8 (bottom) shows. Each channel of the system has two Gunn oscillators, the frequencies of which differ by 10.7 MHz, which is maintained by a phase-locked loop [26]. The microwave beam propagating through the plasma undergoes a change in amplitude and a shift in phase due to the variation of the refractive index $N(R)$ caused by the electron density $n_e(R)$, $N(R) = (1 - n_e(R)/n_e^{crit})^{1/2}$. Here, the plasma electron density is a sum of the equilibrium density and the perturbed density caused by ACs, $n_e(R) = n_0(R) + \delta n(R)$, and

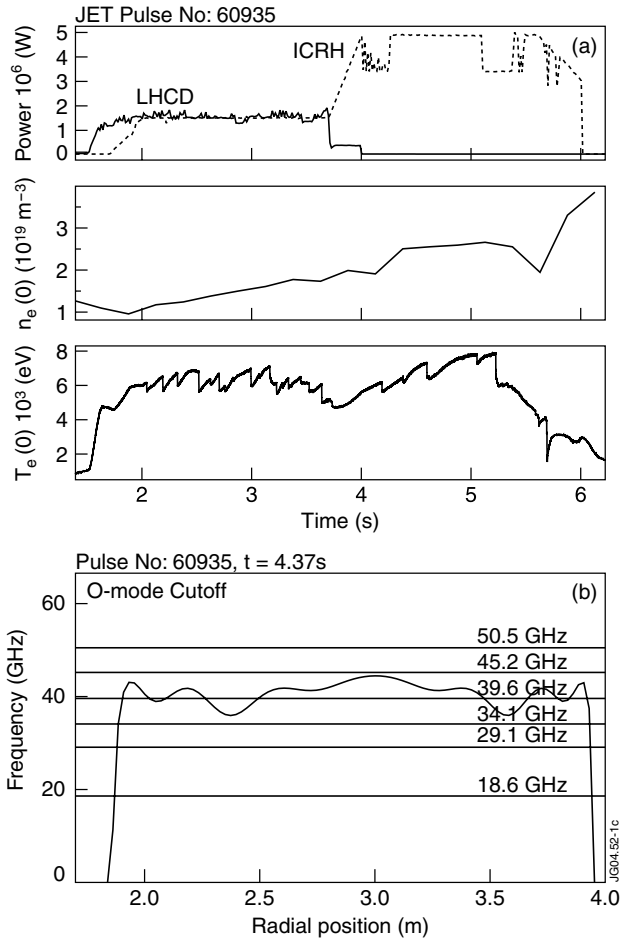

Figure 8. (top) Time evolution of power, density and temperature in JET pulse #60935 and (bottom) O-mode interferometer on JET: microwaves are launched and received at $R = 4$ m; the frequencies of the microwave beams and the O-mode cut-off profile are shown.

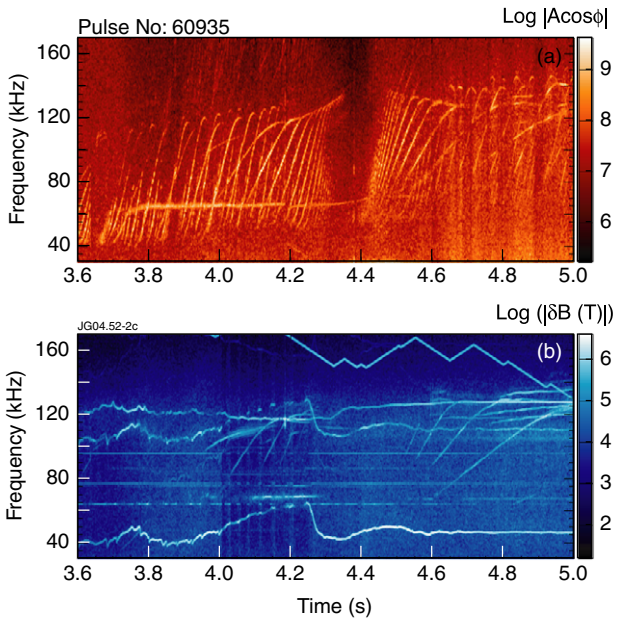

Figure 9. ACs detected in the same discharge with O-mode interferometry (top) and with Mirnov coils (bottom). Microwave beam frequency 45.2 GHz is just above the cut-off frequency as figure 8 (bottom) shows.

n_e^{crit} is the cut-off density determined for microwaves with frequency ω by the condition $\omega = \omega_{pe}$, where ω_{pe} is the plasma frequency. The signals associated with δn are obtained from amplitude A and the change in the phase ϕ of microwave beams caused by the density modulations due to ACs by comparing the beam propagating through the plasma with the reference beam outside the plasma. The beam propagating through the plasma reflects from the inner wall of the torus (at $R \approx 2$ m) in the interferometry regime and from the plasma in the reflectometry regime. The receiver measuring the returned beam is connected to a digital converter with a sampling rate 1 MHz and the data for $A\cos\phi$ and $A\sin\phi$ are recorded with 14 bit effective resolution for 3 s during discharges. Figure 8 (bottom) shows the fixed frequencies of the six-channel microwave beams used in the experiment versus the cut-off frequency determined by the plasma density profile. These beams operated in the interferometry regime if the maximum plasma density was below 0.43×10^{19} m^{-3}, 1.06×10^{19} m^{-3}, 1.44×10^{19} m^{-3}, 1.94×10^{19} m^{-3}, 2.54×10^{19} m^{-3} or 3.16×10^{19} m^{-3}, respectively, for each of the beams above.

While using the interferometry, one measures the line integral of electron density perturbations caused by the AC, δn_{AC}, instead of the edge perturbations of the poloidal magnetic field, $\partial(\delta B_{AC}^{edge})/\partial t$, as in the case of Mirnov coils. Direct comparison of the AC data seen on both the Mirnov coils and on the interferometry signal shows that the interferometry detects a significantly larger number of the ACs as figure 9 (top) and (bottom) shows. The Alfvén frequency spectrum consists of many frequency-sweeping discrete modes observed in the frequency band from 40 kHz to the TAE frequency range, 140 kHz, in agreement with the well-established characteristics of the Alfvén cascades [1]. Figure 9 (top) shows the interferometry measurements of the perturbed density associated with the modes, indicating that very high resolution in both time and frequency with high sensitivity can be achieved, so that ACs with toroidal mode numbers up to $n = 16$ (inferred from the slope $d\omega_{AC}/dt$) are observed. Figure 9 (top) shows that at $t \approx 4.4$ s ACs of all possible mode numbers are excited simultaneously indicating the appearance of $q_{min}(t) =$ *integer* [1], and a clear gap in the density of the ACs observed just before this time shows the depletion (decrease in density) of the rational m/n values as discussed in [27].

A higher frequency, 63.80 GHz, microwave beam was added to the data acquisition for detecting ACs in JET discharges with high NBI power and high plasma density (5×10^{19} m^{-3}), an example of which is shown in figure 10. In discharges with high power NBI-heating, the spectrogram obtained by interferometry, changes significantly as figure 11(*a*) shows. In this case, a significant Doppler shift must be added to the frequency of the AC. Figures 12(*a*) and (*b*) show how the 'lattice' of ACs with different poloidal and toroidal mode numbers changes with increasing toroidal rotation of the plasma. It is seen that all ACs form sets of spectral lines in accordance with their mode numbers. The most important diagnostic event, the grand cascade, is seen as a bunch of modes starting at the same time but with frequencies separated by the Doppler shifts. The depletion of the rational

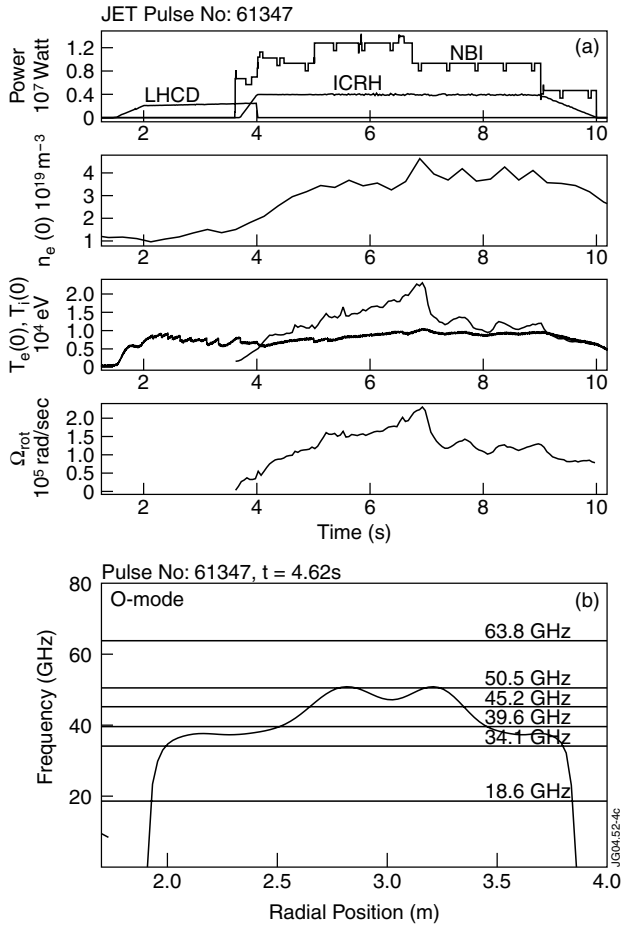

Figure 10. (Top) time evolution of ICRH, NBI and LHCD power, electron density, electron and ion temperatures and toroidal plasma rotation in JET pulse #61347 and (bottom) O-mode interferometer on JET: the frequencies of the microwave beams and the O-mode cut-off profile are shown.

surfaces just before the $q_{\min}(t) = \textit{integer}$ time is still clearly seen before the grand cascade.

3. Grand cascades and ITB triggering events in high density JET plasmas fuelled by NBI only and by NBI and pellets

To examine whether the link between ITB triggering events and low-order rational values of $q_{\min}(t)$ still exists at higher plasma density, JET reversed-shear discharges with NBI-fuelling and deuterium pellets were considered. Grand cascades detected with both interferometry and Mirnov coils whenever possible serve as a primary tool for identifying the $q_{\min}(t) = \textit{integer}$ times. Although the density of plasma in advanced tokamak regimes with NBI heating on JET can be as high as (5.8–6.5) $\times\ 10^{19}\,\mathrm{m}^{-3}$, this high density is usually obtained well after the time of $q_{\min}(t) = 2$, and grand cascades do not occur at this late phase of the discharges. The experimental database, in which grand cascades are observed in discharges with NBI-heating only, covers a much narrower region, up to plasma densities $4.1 \times 10^{19}\,\mathrm{m}^{-3}$ only. In discharges with deuterium pellets added to the NBI fuelling, this AC database expands up to JET plasma density $\sim 5.2 \times 10^{19}\,\mathrm{m}^{-3}$, but only the Mirnov coil signal is available for these discharges.

Considering grand cascades observed at a plasma density $\sim 3 \times 10^{19}\,\mathrm{m}^{-3}$ or more, the times of grand cascades and the times of ITB triggering events were found in all discharges. The triggering event time is determined from the multi-channel ECE measurements of T_e as a sudden change in the slope of $\mathrm{d}T_e/\mathrm{d}t$, such as the one shown in figure 11(*b*). Figure 13 shows that the time of grand ACs still correlates with the time of ITB triggering events within a band of 0.2 s in JET plasmas with densities up to $\sim 5 \times 10^{19}\,\mathrm{m}^{-3}$. The primary uncertainty in figure 13 comes from possibly incorrect 'pattern recognition' for either ACs- or ITB-triggering events, as well as from the error bars for determining the start time of grand ACs, which may be large on the Mirnov coil signal as figure 14 shows. In conclusion, one does not observe any clear weakening or a tendency of weakening of the link between the ITB triggering events and the grand ACs in JET discharges with higher plasma density.

Figure 14 indicates that in most cases grand ACs happen after ITB triggering events. However, the error bars associated with magnetic measurements are too large in some of the high density cases. In order to establish the sequence of events with higher time resolution, interferometry only data points are now taken, and more cases are considered by adding lower density discharges. Figure 15 shows that the high time resolution data still has the same sequence, i.e. the ITB triggering events are observed before grand ACs. For most cases, the ITB triggering occurs at the beginning of the gap in rational surfaces. All the discharges in figure 15 were taken from a similar sequence of pulses with nearly equal rates of evolution of the q-profile. In this figure, the two discharges where the ITB triggering events occur after grand ACs are affected by sawtooth-like events, which probably delay the ITB formation. This shows that the improved plasma confinement in most cases coincides in time with 'gaps' in rational surfaces but not with the presence of $q_{\min}(t) = \textit{integer}$ magnetic surfaces in the plasma. Although the unambiguous identification of the physics effect causing the close link between ITB triggering events and $q_{\min}(t) = \textit{integer}$ times is yet to be found, the observation above seems to support the mechanism of 'depletion' of rational surfaces (see, e.g. [27] and references therein).

4. NBI-driven Alfvén cascades on JET

It was discovered on JET that ACs can also be excited by NBI-produced energetic ions with sub-Alfvénic velocities as low as $V_{\|\mathrm{NBI}} \approx 0.2 \cdot V_A$. Figure 16 shows an example of such NBI-driven ACs. The following characteristic features are important for interpreting these modes. First, spectral lines of these modes are restricted mostly to the lowest frequency part of ACs. Second, modes with higher toroidal mode numbers, n, are seen at higher frequencies, possibly indicating that a trapped particle drift precession resonance is playing a role in exciting these ACs. Third, although these modes are not seen with Mirnov coils and therefore no mode numbers could be determined, from the estimate given by equation (2) one finds that the mode numbers of these NBI-driven ACs, $n \geqslant 7$ ($m \geqslant 20$ for $q_{\min}(t) \sim 3$), are higher than typical mode numbers of ICRH-driven ACs, $1 \leqslant n \leqslant 7$ [1].

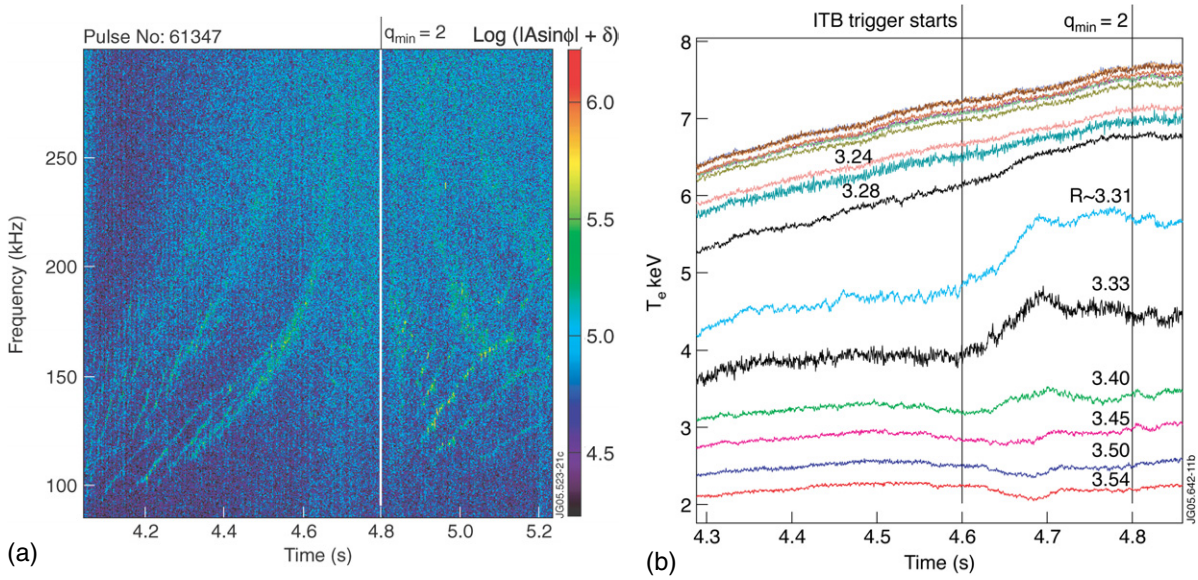

Figure 11. (*a*) ACs detected with the interferometry in JET discharge #61347. Microwave beam frequency 63.8 GHz is above the cut-off frequency ∼50 GHz as figure 10 (bottom) shows. These ACs are not seen on Mirnov coils. A grand cascade is seen at $t \sim 4.8$ s. (*b*) Electron temperature traces measured with multi-channel ECE in JET discharge #61347. An ITB triggering event is seen at $t \sim 4.6$ s.

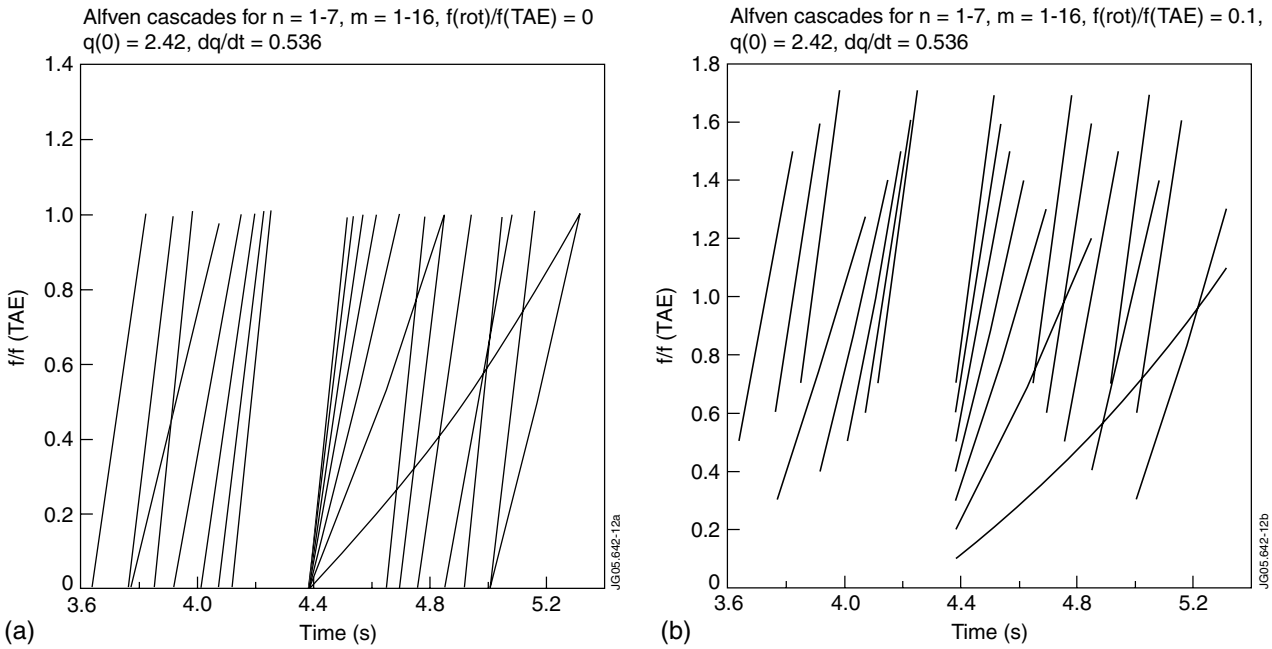

Figure 12. (*a*) Lattice of ACs with toroidal and poloidal mode numbers, $n = 1$–7; $m = 1$–16 described by equation (1) with $\Delta\omega = 0$ in non-rotating plasma corresponding to the case shown in figure 8 (top). (*b*) ACs with $n = 1$–7, $m = 1$–16 in toroidally rotating plasma, with toroidal rotation frequency $\Omega_{rot} = 0.1 \cdot \omega_{TAE}$.

Twenty discharges with NBI-driven ACs were identified, with NBI power as low as 1 MW only (JET pulse #61216). Most of the discharges had low plasma current, $I_P < 1.5$ MA, and high toroidal magnetic field, $B_T = 3.45$ T. Rare exceptions were (1) a discharge with low field $B_T/I_P = 1.25\,\mathrm{T}/1.1\,\mathrm{MA}$ (#62023) and (2) a discharge with higher current, $B_T/I_P = 3.45\,\mathrm{T}/2\,\mathrm{MA}$ (#62752). LHCD with power from 1.2 to 3 MW was used in all cases; only one discharge had no LHCD power (JET pulse #61493). In all the discharges during the observation of NBI-driven ACs the safety factor was quite high, $q_{min}(t) \sim 3$, with one exception (#61498, $q_{min}(t) \sim 2$ at $t \sim 7$ s). Due to the relatively low power of NBI used in these experiments, no significant toroidal plasma rotation was present in these discharges.

The observation of NBI-driven ACs makes diagnostic applications based on ACs much easier since there is no need for generating the super-Alfvénic ions that are usually required for exciting shear-Alfvén modes, such as TAEs [2]. However, an understanding is required as to why the NBI-driven ACs do not experience strong ion Landau damping and what is the

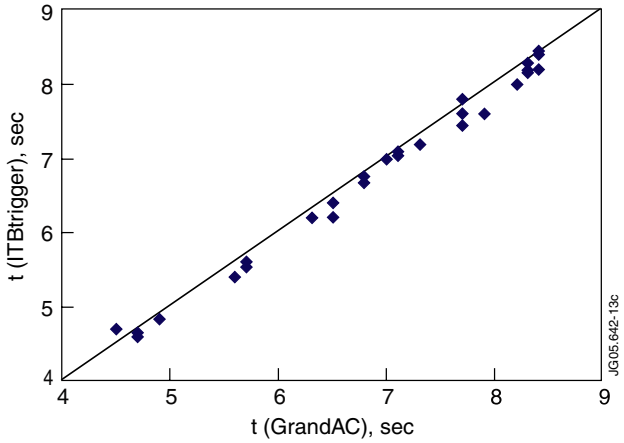

Figure 13. Grand ACs versus ITB triggering events in JET discharges with plasma density at the observation time of $3 \times 10^{19}\,\mathrm{m}^{-3} < n_e(0) < 5.2 \times 10^{19}\,\mathrm{m}^{-3}$.

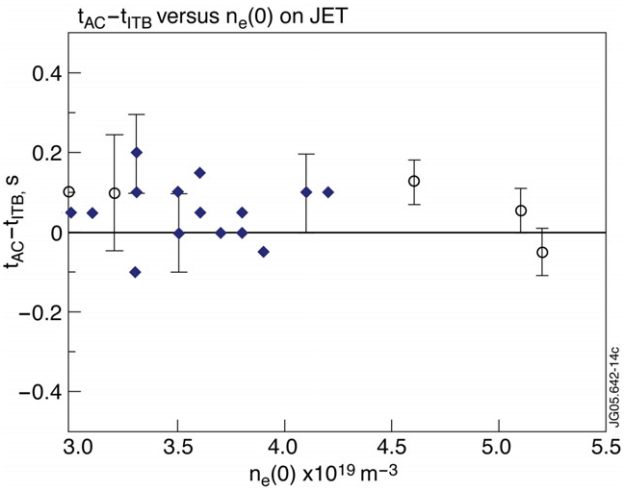

Figure 14. Time delay between grand cascades and ITB triggering events for JET discharges considered in figure 13. A positive value of the time delay shows that an ITB triggering event happens before a grand cascade. Circles represent discharges with pellet fuelling. Typical error bars associated with Mirnov coil signals are shown.

resonance condition for driving these modes by beam ions? In answering the last question, it is important to consider whether any other threshold in the beam velocity exists for exciting these AC modes.

Although the proper explanation of the NBI-driven ACs does require a dedicated experimental and theoretical study, one can pay attention to some features of these modes that may be important for further developments in this area. In particular, since these modes are seen at very low frequency, and the shear Alfvén continuum is deformed at low frequency by the geodesic perturbation of thermal plasma pressure and the coupling to the acoustic waves [9], the equation describing the continuum takes the form (to be compared with equation (1))

$$\Omega^2 - 4(m - nq_{\min})^2 - 4q^2 \frac{C_S^2}{V_A^2}[2 - I_S^+ - I_S^-] = 0. \qquad (3)$$

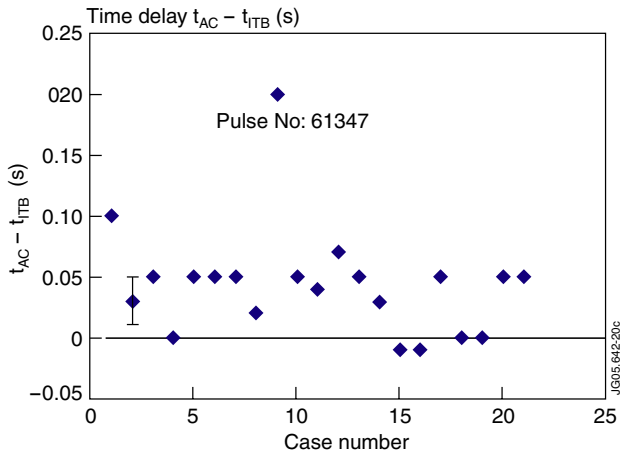

Figure 15. Time delay between grand ACs and ITB triggering events for a set of discharges with interferometry diagnostic used for AC detection, which gives small error bars on AC timing. A positive value of the time delay shows that an ITB triggering event happens before a grand cascade.

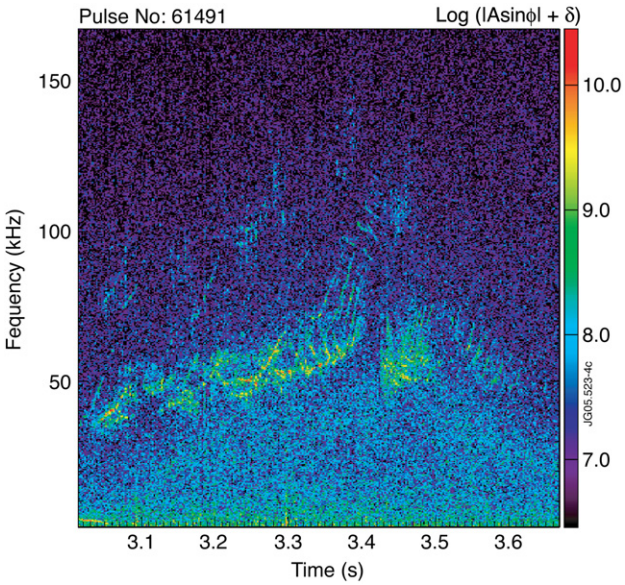

Figure 16. Example of NBI-driven ACs detected with O-mode interferometry in JET pulse #61491 with $B_T = 3.45\,\mathrm{T}$, $I_P \leqslant 2\,\mathrm{MA}$ ($I_P \sim 1.6\,\mathrm{MA}$ at the time of observation). These modes are not seen on Mirnov coils. ACs in this case had highest amplitude amongst all other cases with NBI-driven ACs, with estimated $\delta n_{AC}/n_0$ up to 1% at high magnetic field side. Microwave beam frequency is 45.2 GHz; the cut-off frequency is ~30 GHz.

Here, $\Omega = (2\omega q R_0)/V_A$ is the continuum frequency normalized to the centre-of-TAE gap frequency, $C_S^2 = (T_e + (7/4)T_i)/M_i$ is the ion sound speed and

$$I_S^{\pm} = \frac{4(C_S/V_A)^2(nq_{\min} - m \pm 1)^2}{-\Omega^2 + 4(C_S/V_A)^2(nq_{\min} - m \pm 1)^2}.$$

When the minimum value of the safety factor $q_{\min}(t)$ becomes rational and it satisfies $m - nq_{\min}(t) = 0$, the geodesic term alone determines the minimum continuum frequency,

$$\Omega^2_{\mathrm{Geodesic}} = 8q^2_{\min}\frac{C_S^2}{V_A^2}, \qquad (4)$$

while the coupling to acoustic wave becomes important at

$$\Omega^2_{\text{Acoustic}} = 4\frac{C_S^2}{V_A^2}. \tag{5}$$

Comparison of equations (4) and (5) shows that for typical values of the safety factor in the cases considered, $q_{\min}(t) \sim 3$, the minimum frequency determined by the toroidal coupling to the acoustic mode, Ω_{Acoustic}, is well below Ω_{Geodesic} as $2q^2_{\min} \gg 1$. Since the geodesic compressibility occurs without plasma displacement along the equilibrium magnetic field, the phase velocity of waves at frequency $\geqslant \Omega_{\text{Geodesic}}$ is greater than the ion thermal velocity at $T_e \approx T_i$, and no strong ion Landau damping exists for such modes.

Considering now the resonance conditions for the mode interacting with NBI-produced ions with finite width of drift orbits, one can see that due to the geodesic deformation the passing NBI ions satisfy resonance conditions (including the side-band resonances of higher order caused by the finite orbit effect):

$$\omega_{\text{AC}} \approx \omega_{\text{Geodesic}} = \sqrt{2}\frac{C_S}{R} = V_{\|\text{NBI}}\left(k_\| \pm \frac{p}{qR}\right),$$
$$p = 0, {}_1, {}_2, \ldots. \tag{6}$$

This implies that there is a threshold velocity for the passing NBI-produced ions to drive the mode,

$$\frac{\sqrt{2}}{p} q_{\min} C_S \cong \frac{1}{p} 4 \times 10^6\,\text{m s}^{-1} \leqslant V_{\|\text{NBI}}$$
$$\cong 2 \times 10^6\,\text{m s}^{-1} < V_A \cong 1.3 \times 10^7\,\text{m s}^{-1}, \tag{7}$$

but the velocity threshold is determined by the ion sound speed with factor $\sqrt{2}q_{\min}/p$ and not by the Alfvén speed.

With the NBI line-of-sight directed at $\sim 52^0$ and 64^0 with respect to the magnetic axis (see figure 5), a significant population of trapped NBI-produced ions can also resonate with AC modes typically localized at $r/a \approx 0.3$, where $q_{\min}$ is often localized in JET reversed-shear plasmas. For an effective wave-to-particle energy exchange, the trapped NBI-produced ions should satisfy the drift precession resonance condition,

$$\omega_{\text{AC}} \approx \omega_{\text{Geodesic}} = \sqrt{2}\frac{C_S}{R} \cong n q_{\min} \frac{V^2_{\text{NBI}}}{\omega_{\text{BD}} R r}. \tag{8}$$

This gives a threshold condition for the beam velocity,

$$C_S \left(\frac{r/\rho_S}{n q_0}\right)^{1/2} \leqslant V_{\text{NBI}} \ll V_A, \tag{9}$$

where $\rho_S = C_S/\omega_{\text{Bi}}$. Equation (9) is again determined by the ion sound speed similarly to equation (9) and it gives a quantitative estimate close to equation (9). However, equation (9) does show that the threshold depends on the toroidal mode number of the AC mode, and this may explain the experimental observation that NBI-driven ACs with higher mode numbers achieve higher frequencies.

With the use of the interferometry, it was possible to estimate the amplitude of the NBI-driven modes in the discharge shown in figure 16. It was found that the perturbed density associated with an AC mode in this case corresponds to $\delta n_{\text{AC}}/n_0 \approx 0.25\%$ at the low magnetic field side and $\delta n_{\text{AC}}/n_0 \approx 1\%$ at the high field side. The question then arises whether the NBI-driven ACs may cause a redistribution of NBI-produced ions. JET experiments with tritium NBI-blips into reversed-shear plasma with NBI-driven ACs have been performed and analysed.

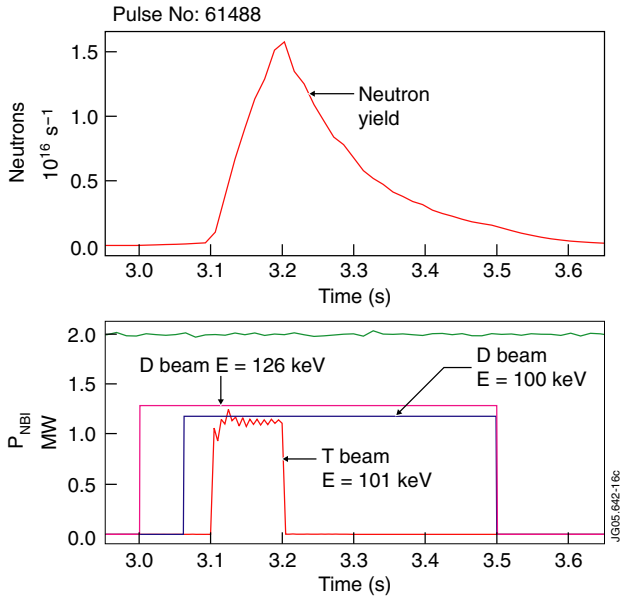

Figure 17. Tritium NBI-blip experiment: time evolution of neutron yield R_{nt} and NBI power from D and T NBI sources in JET discharge #61488 with $B_T = 3.45$ T, $I_P \leqslant 2$ MA.

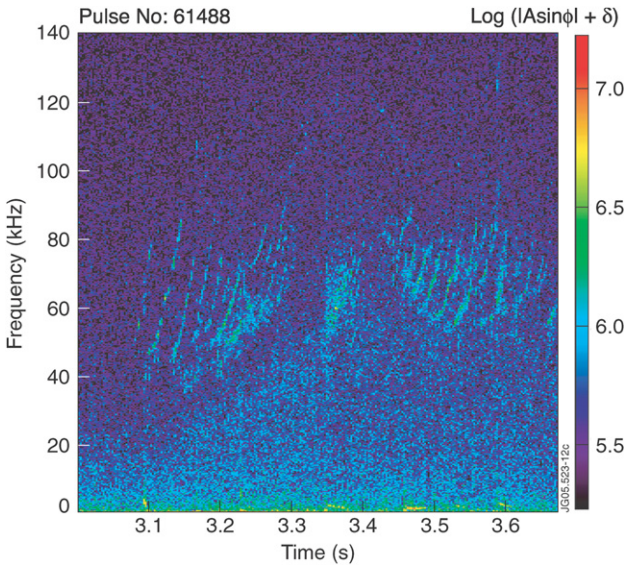

Figure 18. ACs observed with O-mode interferometry at the time of T-NBI blip in JET discharge #61488. Plasma current is $I_P \sim 1.6$ MA at the time of observation. Microwave beam frequency is 39.6 GHz; the cut-off frequency is ~30 GHz.

Figure 17 shows the set-up of this experiment performed during the 2003 tritium trace campaign on JET. First, low power deuterium NBI is injected into a deuterium plasma and the NBI-produced ions excite ACs, which are shown in figure 18. In addition to the deuterium NBI, a short blip of tritium NBI is applied in order to generate a very significant yield of DT neutrons born in beam-plasma reactions and to observe whether the dynamics of neutron decay indicates any

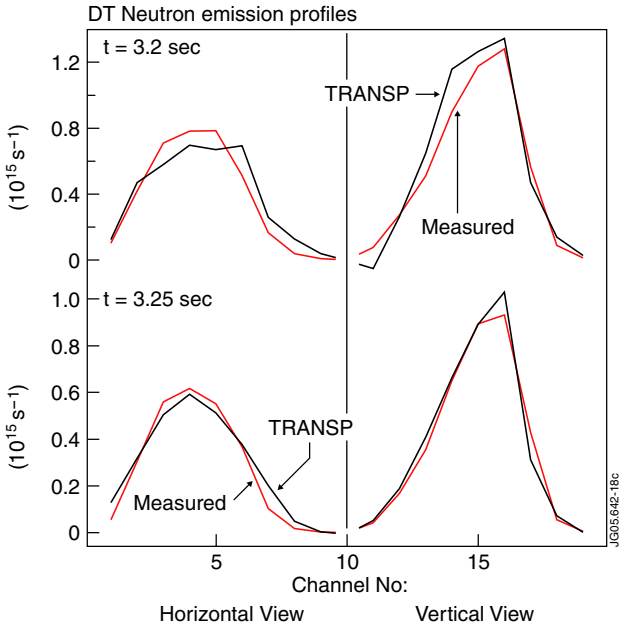

Figure 19. The TRANSP code modelling based on Coulomb collisions alone versus DT neutron profiles for discharge #61488. Channels 1–10 show the horizontal view neutron camera measurements (from top (channel 1) to bottom (channel 10)); channels 11–19 show the vertical view neutron camera measurements (from high field side channel 11 to low field side channel 19).

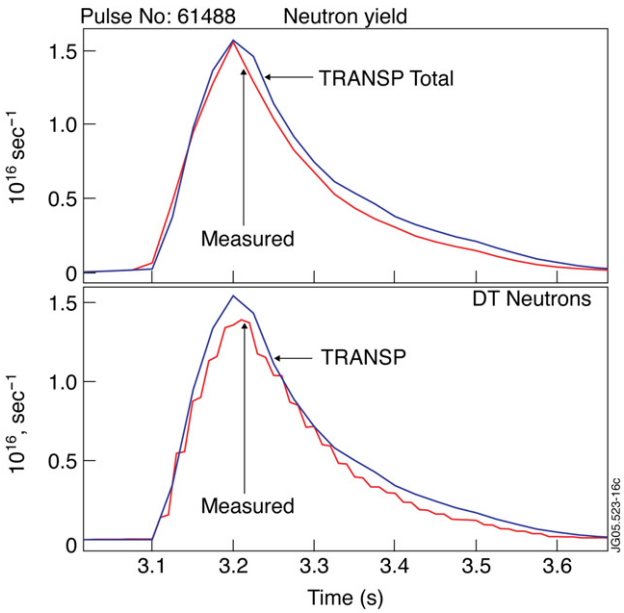

Figure 20. The TRANSP code modelling of neutron yield temporal evolution versus the measured total neutron yield for discharge #61488. The top box shows the total neutron yield due to both DD and DT neutrons; the bottom box shows DT neutrons only.

anomalous radial transport of the tritium NBI. Figures 19 and 20 show how the measured beam–plasma neutron yield compares with the neutron yield predicted with the TRANSP code [28] that uses classical collisional transport and $Z_{\rm eff}$ measurements from the horizontal view spectroscopy (error bars of ∼30%). A good correlation is found in this discharge between the calculated collisional transport and measured neutron profiles, for both neutron measurements from DD and DT reactions. This good correlation in both time evolution and in the profile shape shows that in this discharge the NBI-driven ACs do not cause any notable deviation from the classical transport of the NBI-produced ions.

5. Conclusions

In order to investigate the Alfvén cascade eigenmodes and ITB triggering events in higher-density JET reversed shear plasmas, an interferometry technique for detecting ACs in JET discharges with high power NBI-heating was used, in addition to the detection of ACs with Mirnov coils. The well-established 'low-density' correlation between grand ACs and ITB triggering events was found to persist within a band of $\leqslant 0.2$ s up to densities 4.1×10^{19} m^{-3} in NBI-only discharges and up to densities 5.2×10^{19} m^{-3} in JET discharges fuelled by NBI and deuterium pellets. In order to establish the sequence of ITB triggering events and grand cascades with high time resolution, interferometry-only data were taken for the AC detection, and more cases were considered by adding lower density discharges. The ITB triggering events were found to occur in most cases just before grand ACs, thus suggesting that the spontaneous improvement in plasma confinement is associated with the effect of rational surface depletion just before $q_{\rm min}(t) = \textit{integer}$ times, rather than with the presence of the integer magnetic surfaces in the plasma. NBI-driven ACs were detected with interferometry in JET discharges with low NBI power and with high values of the safety factor, $q_{\rm min} \approx 3$. Analysis presented in this paper indicates that the observed NBI-driven ACs determined at lowest frequency by the geodesic acoustic effect may indeed have a low thermal ion Landau damping and may be driven by both passing and trapped NBI-produced ions with velocities exceeding a certain threshold associated with the ion sound speed below the Alfvén speed. NBI-driven ACs were observed during JET tritium NBI blip experiments when the high neutron rate was used for probing the tritium beam transport. It was found that even in the presence of ACs the measured DT neutron profiles and total neutron yields agree well with the TRANSP code modelling based on Coulomb collisions indicating that the ACs had no significant effect on fast ion confinement in the case considered.

Acknowledgments

The authors would like to thank their colleagues at JET who operated the tokamaks, the heating systems and the diagnostics during these experiments. The work was performed under the European Fusion Development Agreement and was partly funded by Euratom and the UK Engineering and Physical Sciences Research Council. The views and opinions expressed herein do not necessarily reflect those of the European Commission.

References

[1] Sharapov S.E. *et al* 2002 *Phys. Plasmas* **9** 2027
[2] Borba D.N. *et al* 2000 *Nucl. Fusion* **40** 775

[3] Sharapov S.E. *et al* 2001 *Phys. Lett.* A **289** 127
[4] Berk H.L. *et al* 2001 *Phys. Rev. Lett.* **87** 185002
[5] Sharapov S.E. *et al* 2004 *Phys. Rev. Lett.* **93** 165001
[6] Nazikian R. *et al Proc. 20th Int. Conf. on Fusion Energy 2004 (Vilamoura, Portugal, 2004)* (Vienna: IAEA) paper EX/5-1 http://www-naweb.iaea.org/napc/physics/fec/fec2004/datasets/index.html
[7] Cheng C.Z., Chen L. and Chance M.S. 1985 *Ann. Phys. (N.Y.)* **161** 21
[8] Sharapov S.E., Mikhailovskii A.B. and Huysmans G.T.A. 2004 *Phys. Plasmas* **11** 2286
[9] Breizman B.N., Berk H.L., Pekker M.S., Pinches S.D. and Sharapov S.E. 2003 *Phys. Plasmas* **10** 3649
[10] Breizman B.N., Pekker M.S. and Sharapov S.E. 2005 *Phys. Plasmas* **12** 112506
[11] Kimura H. *et al* 1998 *Nucl. Fusion* **38** 1303
[12] Shinohara K. *et al* 2004 *Plasma Phys. Control. Fusion* **46** S31
[13] Snipes J.A. *et al* 2005 *Phys. Plasmas* **12** 056102
[14] Nazikian R. *et al* 2003 *Phys. Rev. Lett.* **91** 125003
[15] Van Zeeland M.A. *et al* 2005 *Plasma Phys. Control. Fusion* **47** L31
[16] ITER Physics Basis 1999 *Nucl. Fusion* **39** 2137
[17] Goedbloed J.P. *et al* 1993 *Plasma Phys. Control. Fusion* **35** B277
[18] Fasoli A. *et al* 2002 *Plasma Phys. Control. Fusion* **44** B159
[19] Young N. *et al* 2006 *Plasma Phys. Control. Fusion* **48** 295
[20] Joffrin E. *et al* 2003 *Nucl. Fusion* **43** 1167
[21] Challis C.D. *et al* 2001 *Plasma Phys. Control. Fusion* **43** 861
[22] Hawkes N.C. *et al* 2001 *Phys. Rev. Lett.* **87** 115001
[23] Austin M.E. *et al* 2006 Core barrier formation near integer q surfaces in DIII-D *Phys. Plasmas* **13** at press
[24] Van Zeeland M.A. 2006 *9th IAEA TCM on Energetic Particles (Takayama, Japan, 2005) Nucl. Fusion* **46** S880
[25] Hacquin S. *et al* 2006 Characterisation of Alfvén cascades on the JET tokamak using a multi-channel O-mode reflectrometry diagnostic *Nucl. Fusion* **46** S714
[26] Sips A.C.C. and Kramer G.J. 1993 *Plasma Phys. Control. Fusion* **35** 743
[27] Garbet X. *et al* 2003 *Nucl. Fusion* **43** 975
[28] Budny R.V. *et al* 1992 *Nucl. Fusion* **32** 429